Electronic Journal of Structural Engineering

Original Article

Cite this: DOI:10.56748/ejse.25634

Received Date: 06 May 2024
Accepted Date: 08 January 2025

1443-9255
https://ejsei.com/ejse

Three-dimensional discrete element analysis of the excavation face stability of deep-buried shield tunnels

Xin Huang[a,b,c], Zihao Zhang[a] , Guangyi Yan[d*], Jiaqi Guo[a,c], Chong Xu[d] , Qi Liang[a]

[a] School of Civil Engineering, Henan Polytechnic University, Jiaozuo, Henan 454003, China
[b] Shandong University, Jinan, Shandong, 250061, China
[c] Collaborative Innovation Center of Coal Work Safety and Clean High Efficiency Utilization, Jiaozuo, Henan, 454003, China
[d] China Railway First Survey and Design Institute Group Co., Ltd., Xian, Shanxi, 710043, China
*Corresponding author: 3637226920@qq.com

Abstract

To study the stability and the influencing factors of shield tunnel excavation face under deep burial conditions, relying on the Bailuyuan shield tunnel in the second phase of the "Water Diversion from the Han to the Wei River" project, we conducted indoor uniaxial compression tests, repose angle tests, and three-dimensional discrete element simulation analysis, calibrated the microparameters of the strata, and constructed a three-dimensional discrete element model of shield tunnel excavation face. The stability and settlement characteristics of the shield tunnel excavation face under different influencing factors were studied. Research results showed that the buried depth of the tunnel has a significant effect on the horizontal displacement of tunnel excavation face and the critical chamber earth pressure ratio, followed by the cutterhead opening rate, belong to the main influencing factors. The excavation speed has no obvious effect on the critical chamber earth pressure ratio. The rotation speed of the cutterhead has little effect on the settlement of the strata, belonging to the secondary influencing factors. In the actual construction, the excavation speed mainly affects the settlement of the strata, and the cutterhead opening rate mainly affects the stability of the shield itself.

Keywords

Deep-buried shield tunnel, Excavation face stability, Chamber earth pressure, 3D discrete element analysis

1. Introduction

With the rapid development of infrastructure construction and transportation engineering in China, the extensive utilization of underground space has become a trend (Ge et al. 2023). In the construction of underground tunnels, shield tunneling is widely used due to its advantages of fast construction speed, low environmental impact, and strong geological adaptability. There is a significant difference in the stability of the excavation face between deep-buried shield tunnels and shallow-buried ones. A deep-buried tunnel increases the likelihood of encountering adverse geology, both in terms of depth along the longitudinal direction and breadth along the tunnel axis. The instability of the excavation face seriously affects the safety of tunnel construction, induces large-scale landslides, causing machine jamming and even loss of life and property (Su et al. 2019; Dong et al. 2019). Therefore, conducting research on the stability of the excavation face of deep-buried shield tunnels has significant theoretical and practical significance.

Scholars at home and abroad have conducted extensive research on the stability of shield tunnel excavation faces. Ibrahim et al. (2015) used Midas-GTS software to study the failure mode of excavation faces in soft earth layers, revealing the three-dimensional failure mode of excavation face of earth pressure balance shield tunneling in soft earth layers. Lu et al. (2023) proposed a machine learning method based on heuristic optimization algorithm to predict the ground displacement caused by earth pressure balance shield tunneling through on-site measurement and model analysis. Li et al. (2023) carried out a study on the effect of formation inclination angle on the stability of tunnel excavation face by combining theoretical analysis and numerical simulation. Fu et al. (2022) proposed an optimized genetic algorithm back propagation neural network (BPNN-GA) for reasonable selection of operating parameters and accurate ar prediction to determine the optimal selection of various influencing parameters to maintain the stability of the excavation face. Liu et al. (2022) studied the influence of factors such as tunnel burial depth, cutterhead opening ratio, and advancing speed on the stability of excavation face using finite difference software FLAC3D based on orthogonal experiments. Based on examples of excavation face instability, Yao et al. (2023) conducted a three-dimensional discrete element analysis on the causes and development process of excavation face instability, and combined with measured data, proposed a stability control method for excavation faces. Qi et al. (2023) conducted geomechanically model experiments and numerical simulations to study the effect of chamber earth pressure on the unstable area of excavation face under different burial depths of tunnels.

Yang et al. (2016) employed the Plaxis8.2 finite element calculation software to investigate the influences of factors such as the internal friction angle, water head height, tunnel burial depth, and tunnel diameter on the stability of the excavation face. Niu et al. (2023) analyzed the influence of excavation parameters such as jacking force, cutting speed and soil conditions on the stability of excavation face by numerical simulation. Chen et al. (2023) Based on FLAC3D numerical simulation software, the ultimate support pressure and safety factor were used as the evaluation criteria for the stability of the excavation face to analyze the internal friction angle, cohesion, and hole diameter to the stability of the excavation face. Xu et al. (2023) Through a combination of numerical simulations and experimental analyses, the impact of various parameters, including support pressure, and cutters on the stability of the excavation face were explored.

Hernandez et al. (2019) used the numerical method of ABAQUS three-dimensional finite element software to study the influence of soil parameters and tunnel width on the stability of excavation face of shallow tunnel. Based on the upper bound theorem of limit analysis, Zhang et al. (2019) established different failure models of shallow tunnel working face instability and analyzed the influence of tunnel buried depth and tunneling speed on stability. Through theoretical analysis, numerical simulation and comprehensive study of field monitoring data, Li et al. (2019) deeply discussed the influence of tunnel shape, size, buried depth, excavation method and construction speed on the stability of shallow tunnel excavation face. Through numerical simulation and model test, Wang et al. (2023) analyzed the influence of parameter design, stress release during excavation and disturbance during construction on the stability of shallow tunnel excavation face. Through practical engineering cases, Chen et al. (2022) discussed how to improve the stability of the excavation surface of shallow tunnels through construction parameter optimization and construction factor control.

The above research is of great significance for guiding the stability control and safe construction of shallow-buried shield tunnel excavation faces. With the continuous development of underground engineering downward, the impact of large burial depth on shield tunneling excavation cannot be ignored. For example, the burial depth of the Bailuyuan Tunnel in the “Water Diversion from the Han to the Wei River” project has reached 270-300 m. At present, there are few research on the influence of different factors on the excavation face of shield tunnels under deep burial conditions, especially the construction parameters such as cutterhead

opening ratio, excavation speed, cutterhead speed, and chamber earth pressure that are directly related to the stability of the excavation face.

Take the Bailuyuan Tunnel in the second phase of the "Water Diversion from the Han to the Wei River" project as the engineering case, the microscopic parameters of the strata were calibrated by us through conducting uniaxial compression and repose angle indoor tests; meanwhile, a three-dimensional discrete element model of the interaction between shield tunneling and strata was established by us for further analysis. The aim is to study the changes in excavation face displacement and strata settlement caused by different influencing factors such as tunnel burial depth, cutterhead opening ratio, shield tunneling speed, and cutterhead speed under different chamber earth pressures, and to determine the critical pressure of the chamber earth under different working conditions. The research results can provide reference for the stability control of surrounding rock and optimization of excavation parameters for deep-buried shield tunnels.

2. Construction of Three-Dimensional Discrete Element Model

2.1 Uniaxial compression test and repose angle test were used to calibrate the microscopic parameters of the rock sample

The microscopic parameters of the rock sample are calibrated by using a uniaxial compression test and repose angle test. The rock and loose earth samples were taken from the site of the Bailuyuan Tunnel. The lithology is argillaceous sandstone, with a density of 2060 kg/m3, a natural water content of 17.6%, a Poisson's ratio of 0.17, and a shear modulus of 1×108 Pa.

Process the sample into a cylindrical specimen of 50 mm × 100 mm for uniaxial compression testing, and use the method of controlling displacement for loading at a loading rate of 2 mm/s. Record the instantaneous stress and test curve during the experiment, with a counting interval of 0.12 s. Load until the specimen fails, as shown in Fig. 1 (a), the peak load of the rock sample is 2.79 MPa. Use a repose angle tester to measure the repose angle of loose earth samples. Add the loose earth sample to the funnel and stir it to ensure that the material falls evenly onto the tray. Repeat the experiment three times in a unified manner. After the scattered earth sample falls completely and stabilizes in the tray, measure the natural repose angle and take the average value, as shown in Fig. 2 (a). After measurement, the repose angle of the earth sample is 41°.

Be based on the results of the uniaxial test and repose angle test mentioned above, numerical uniaxial test and numerical repose angle test were used to calibrate the required microscopic parameters in the EDEM （2020） discrete element model. Since the prototype strata is a soft rock formation with certain viscosity, the Hertz-Mindlin with JKR contact model built in EDEM software was selected as the contact model, and bonding were set between particles to simulate that the sample has a certain strength (Zhang et al. 2023). This contact model is based on Hertz theory and considers the influence of wet particle bonding force on particle motion. It is a cohesive contact model suitable for simulating situations where significant bonding and agglomeration occur between particles due to static electricity, water, and other reasons, such as cohesive earth.

The normal elastic force is based on the overlap and phase surface energy, expressed as:

$$F_{JKR} = \frac{4E^*}{3R^*}\alpha^3 - 4\alpha^{\frac{3}{2}}\sqrt{\pi\gamma E^*} \quad (1)$$

$$\delta = \frac{\alpha^2}{R^*} - \sqrt{\frac{4\pi\gamma\alpha}{E^*}} \quad (2)$$

where F_{JKR} is the normal elastic contact force of JKR, and γ is the surface energy; α is the tangential overlap, and δ is the normal overlap; E* is the equivalent elastic modulus, and R* is the equivalent contact radius. The equivalent elastic modulus and equivalent contact radius can be calculated using the following formula:

$$\frac{1}{E^*} = \frac{1-\nu_1^2}{E_1} + \frac{1-\nu_2^2}{E_2} \quad (3)$$

$$\frac{1}{R^*} = \frac{1}{R_1} + \frac{1}{R_2} \quad (4)$$

where E_1 and E_2 are the elastic moduli of particles 1 and 2, respectively; ν_1 and ν_2 represents the Poisson's ratio of particles 1 and 2, respectively; R_1 and R_2 are the radius of particles 1 and 2, respectively.

Even if there is no direct contact between particles, this model can still provide the cohesive force of mutual attraction between particles. The maximum gap between particles with non-zero cohesion is calculated using the following formula:

$$\delta_c = \frac{{\alpha_c}^2}{R^*} - \sqrt{\frac{4\pi\gamma\alpha_c}{E^*}} \quad (5)$$

$$\alpha_c = \left[\frac{9\pi\gamma {R^*}^2}{2E^*}\left(\frac{3}{4} - \frac{1}{\sqrt{2}}\right)\right] \quad (6)$$

where δ_c is the maximum normal gap between particles with non-zero cohesion, and α_c is the maximum tangential gap between particles with non-zero cohesion. When $\delta < \delta_c$, the model returns 0. When the particles are not in actual contact and the gap is less than δ_c, the cohesion reaches its maximum value. The formula for calculating the maximum cohesion force $F_{pullout}$ of particles in non-actual contact is:

$$F_{pullout} = -\frac{3}{2}\pi\gamma R^* \quad (7)$$

The numerical uniaxial compression test and numerical repose angle test are strictly carried out in accordance with the indoor test procedure. The uniaxial compression test and repose angle test are shown in Fig. 1 (b) and 2 (b).

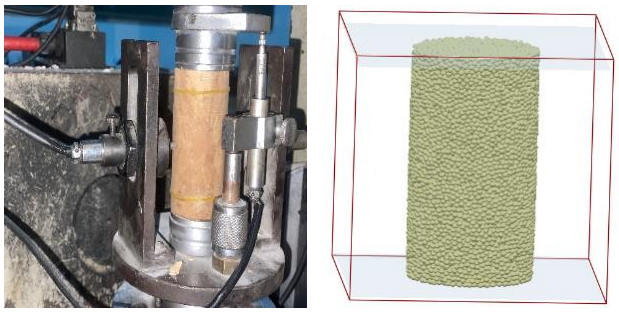

(a) (b)

Fig. 1 Uniaxial compression test; (a) Laboratory test; (b) Numerical simulation

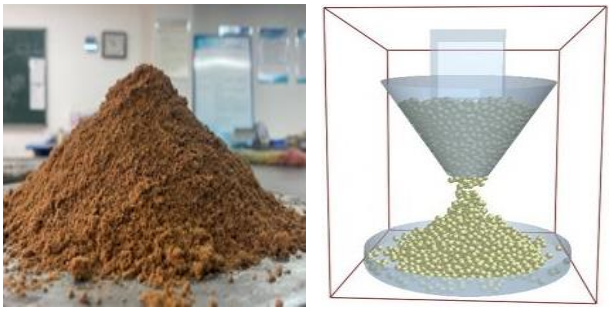

(a) (b)

Fig. 2 Repose angle test; (a) Laboratory test; (b) Numerical simulation

By repeatedly adjusting the microscopic parameters of the discrete element particles for numerical simulations, a comparison between the stress-strain curve of the numerical test and that of the laboratory uniaxial test can be obtained, as shown in Fig. 3. The bulk material slowly flowed into the flat-bottom container from a certain height through the funnel and other tools to form a conical accumulation body. The angle between the slope and the horizontal plane of the conical accumulation body is measured by the protractor, and this angle is the angle of repose. The repose angle of the simulation test was 40.68°. From Fig. 3, the stress-strain curve of the numerical test is in good agreement with that of the laboratory test, and the size of the repose angle in numerical simulation is close to that in laboratory test. The microscopic parameters of the material are determined through numerical experiments as shown in Table 1, and the contact parameters are shown in Table 2.

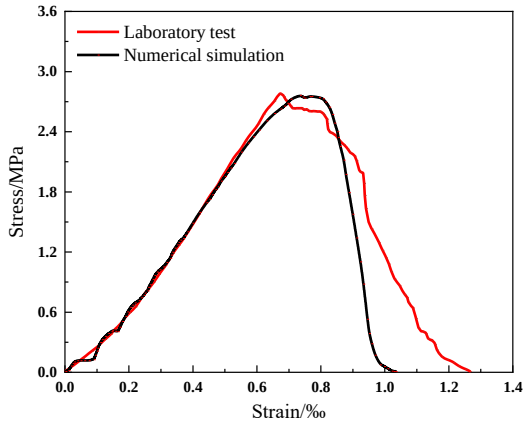

Fig. 3 Stress-strain curves of numerical simulation and laboratory test

Table 1. Micromechanical parameters

Normal contact stiffness (N/m³)	Tangential Contact stiffness (N/m³)	Critical normal stress (Pa)	Critical tangential stress (Pa)
1×10⁸	7×10⁸	5×10⁸	5×10⁸

Table 2. Model contact parameters

Coefficient of static friction	Coefficient of rolling friction	Coefficient of restitution	JKR surface Energy (J/m^2)
0.5	0.5	0.01	7

2.2 Shield machine model

The built-in modeling module of EDEM software cannot meet the three-dimensional modeling requirements of shield tunneling machines, a complex machinery. However, it supports the import of various formats of CAD graphics generated by mainstream three-dimensional modeling software. We took the TBM of the Bailuyuan Tunnel as a prototype and got it appropriately simplified to establish a 3D shield machine model that includes such main structures as cutterhead, earth chamber, screw conveyor and shield shell using the SolidWorks 3D modeling software. Then, we saved the model file as STEP format, imported it into the EDEM 3D discrete element numerical simulation platform. As shown in Fig. 4 (a), the diameter of the cutterhead of the 3D shield machine model is 5,100 mm, the overall length of the shield machine is 6,500 mm, the cutterhead opening rate is 55%, and the inclination angle of the screw conveyor is 36°.

According to the actual movement of the shield machine, in EDEM, it is necessary to control the forward and rotating postures of the cutterhead, shield body, and screw conveyor by setting the motion forms of different components of the shield machine. Fig. 4 presents the motions forms of each component. Therein, all horizontal movements are set along the tunnel axis direction, the cutterhead rotates around its center, and the screw conveyor rotates around itself

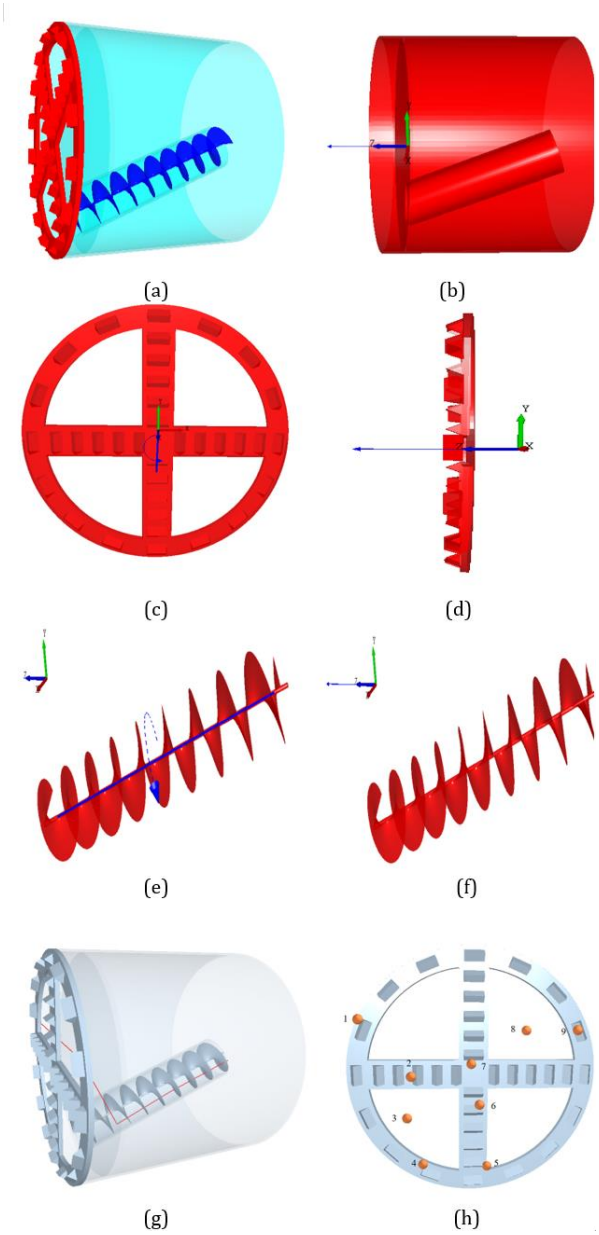

Fig. 4 Shield tunneling model and movement posture of each component; (a) Shield machine model; (b) Horizontal movement of shield; (c) Rotational movement of cutterhead; (d) Horizontal movement of cutterhead; (e) Rotational movement of screw conveyor. (f) Horizontal movement of screw conveyor; (g) Particle trajectory. (h) Particle monitoring

2.3 Three-dimensional discrete element calculation model of shield tunneling

In view of factors such as actual engineering size, calculation time, and particle size, the design of the 3D discrete element model is as follows: the X-axis direction is the tunnel axis direction, the Y-axis direction is the model width direction, and the Z-axis direction is the vertical direction. The model size is 6.1 m × 21 m × 20.5 m. Generate heavy particles in the upper part of the earth to replace ground stress and to simulate the burial depth (300 m) of the prototype tunnel. The height of the heavy particle loading layer is 0.5 m, and the density of heavy particles is 1.12 × 106 kg/m3. The particles in the lower strata are 20 m high, with a density of rock and earth, and a total of 421,183 particles are generated. The excavation face of the shield machine is set in the middle of the cross-section, 7.95 m from the left and right sides of the model, and 7.7 m from the top of the model. The 3D numerical model is shown in Fig. 5. The boundary conditions of the model are the top of the model is set as free and unconstrained, and the other sides are constrained by displacement using the wall element built in the EDEM software.

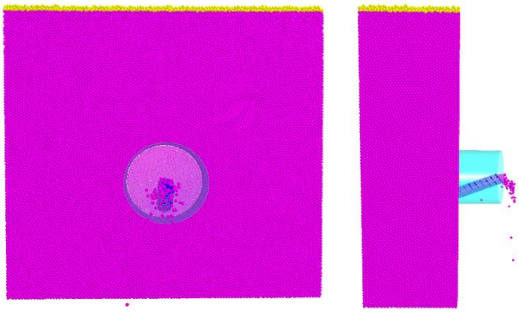

Fig. 5 3D numerical model; (a) Front view; (b) Side view

2.4 Chamber earth pressure control

The magnitude of the support pressure of the chamber earth during shield tunneling is directly related to the stability of the excavation face. Therefore, during the simulation, a monitoring section is set inside the earth chamber to monitor the pressure in real time. According to the monitoring results of chamber earth pressure, the control of the chamber earth pressure can be achieved by changing the speed of the screw conveyor at a specific shield tunneling speed. When the chamber pressure is too high, the speed of the screw conveyor shall increase to accelerate the discharge of soil from the earth chamber; When the chamber pressure is less than the set value, the speed of the screw conveyor shall decline to slow down the discharge of soil inside the earth chamber. By controlling the theoretical earth input and output, the shield tunneling is in dynamic equilibrium and the excavation face is in a stable support pressure state.

At the moment before the instability of the excavation face, the ratio of the pressure in the earth chamber to the transverse ground stress of the excavation face is the critical chamber earth pressure ratio. To investigate the critical chamber earth pressure ratio for maintaining the stability of the excavation face of the shield tunnel under the influence of various factors. During the excavation, first adjust the chamber earth pressure to the design value, that is, the chamber earth pressure ratio is 1; then adjust the rotation speed of the screw conveyor, which will gradually reduce the chamber pressure until the displacement of the excavation face increases sharply, that is, the tunnel excavation face is in a critical state of losing stability. Based on this, the critical chamber earth pressure ratio to maintain the stability of the tunnel excavation face can be obtained.

3. Stability Analysis of Excavation Face of Deep-Buried Shield Tunnel

The stability of the excavation face during shield tunnelling mainly depends on the reasonable control of the chamber earth pressure, which is closely related to factors such as tunnel burial depth, cutterhead opening rate, cutterhead rotation rate, and shield tunneling speed. Therefore, this section studies the influence of these factors on excavation face displacement and stratum settlement under different chamber earth pressures, to determine the critical support pressure of earth chambers under different working conditions and provide reference for the setting of chamber earth pressure in shield tunnels.

To clarify the impact of various factors on the excavation face, only a single variable is changed in each working condition to avoid other factors affecting the results. The monitoring section is set as shown in Fig. 6. Five monitoring sections are set up for the displacement of the excavation face, each with the spacing of 1 m. During the excavation process of each section, the gradient adjustment of the chamber earth pressure is completed to obtain the horizontal displacement of the excavation face at

different chamber pressure ratios; The monitoring section for stratum subsidence is set 3 m above the tunnel. Under stable pressure conditions (λ= 1), when the shield cutterhead reaches Section I, the ground settlement occurs.

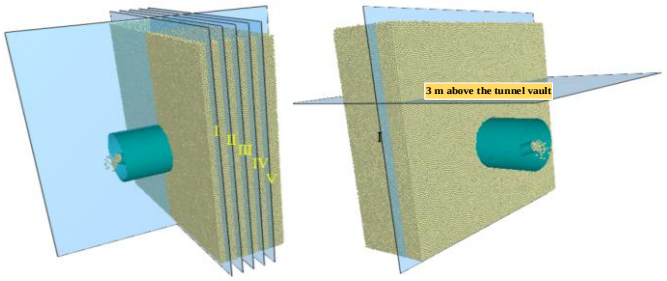

(a) (b)

Fig. 6 Monitoring sections; (a) Monitoring section of excavation face displacement; (b) Monitoring section of ground subsidence

3.1 The influence of tunnel burial depth on the stability of excavation face

The burial depth of the tunnel is taken as 100 m, 200 m, and 300 m, while other factors remain unchanged. The influence of burial depth on the stability of the shield tunnel excavation face is studied. The relationship curve between the horizontal displacement of the excavation face and the variation of the chamber earth pressure ratio under different burial depths is shown in Fig. 7.

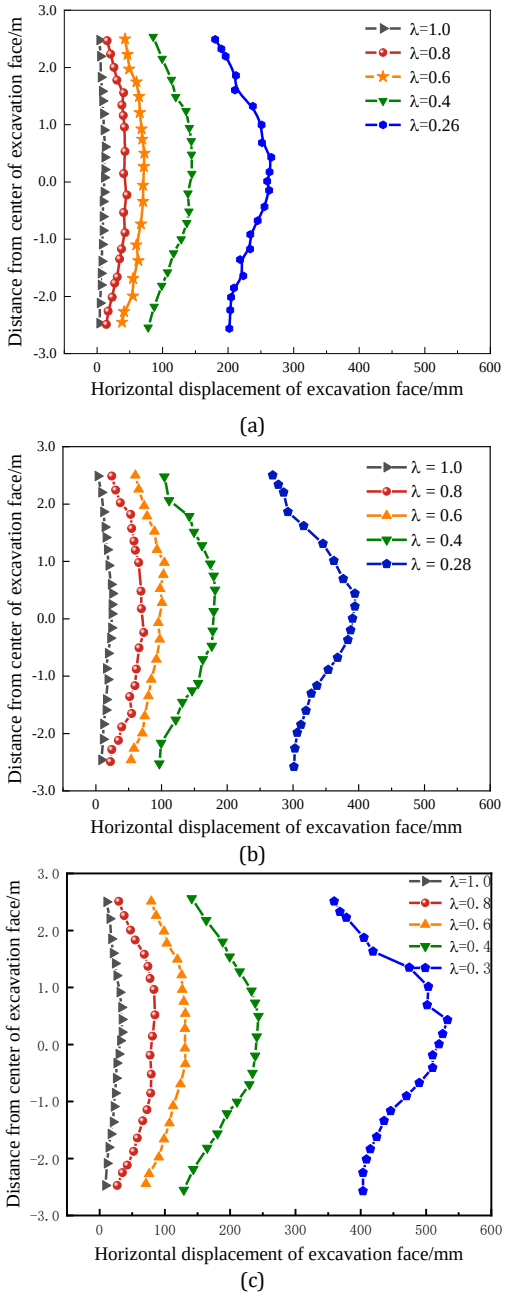

Fig. 7 Deformation of excavation face under different burial depths. (a) 100 m; (b) 200 m; (c) 300 m

From Fig. 7, as the chamber earth pressure ratio decreases, the deformation of the excavated earth towards the chamber gradually increases, and the horizontal displacement of the upper excavation face is slightly greater than that of the lower part. The maximum earth displacement occurs above the center point of the tunnel. The overall curve shows a large displacement in the middle part and a small displacement at the upper and lower ends. Under the same chamber earth pressure ratio, as the burial depth increases, the displacement of the excavation face increases. The critical chamber earth pressure ratios at burial depths of 100 m, 200 m and 300 m are 0.26, 0.28 and 0.3, respectively. This means that as the burial depth increases, the critical chamber earth pressure ratio required to stabilize the excavation face also increases, indicating the deeper the tunnel is buried, the greater the deformation of the excavation face, and the poorer the stability.

The relationship between the maximum horizontal displacement of the excavation face and the chamber earth pressure under different burial depths is shown in Fig. 8.

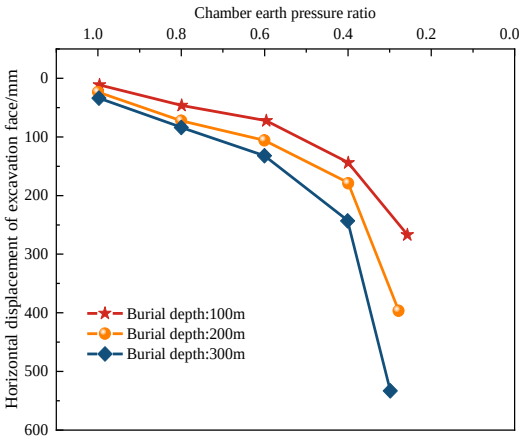

Fig. 8 Relationship between maximum horizontal displacement of excavation face and the chamber earth pressure ratio under different burial depths

As shown in Fig. 8, under the same burial depth, as the chamber earth pressure ratio decreases, the overall horizontal displacement of the excavation face shows a three-stage trend: Stage I - the chamber earth pressure ratio is 1~0.6, the horizontal displacement of the excavation face slowly increases with the decrease of the pressure ratio, and the excavation face is in a relatively stable state; Stage II - the pressure ratio is 0.6~0.4, the increase in horizontal displacement of the excavation face increases compared to Stage I, indicating that the earth displacement is more sensitive to changes in the chamber pressure. At this point, the chamber earth pressure should be increased to prevent the excavation face losing stability; Stage III - the pressure ratio is less than 0.4, although the earth pressure does not change much, the horizontal displacement of the excavation face increases sharply. At this point, the excavation face is already in an unstable state, and the corresponding value is the minimum critical chamber earth pressure. In addition, as the burial depth increases, the horizontal displacement of the tunnel excavation face shows a non-linear growth. Under different burial depths, the smaller the pressure ratio, the greater the difference in displacement of the tunnel face.

3.2 The influence of cutterhead opening rate on the stability of excavation face

The cutterhead opening rates of shield tunneling are set to 45%, 55% and 65%, the burial depth of the tunnel is taken as 300m, while other factors remain unchanged. The influence of cutterhead opening rates on the stability of the excavation face of shield tunneling is studied. The compressive force on the excavation face earth under different cutterhead opening rates is shown in Fig. 9.

From Fig. 9, the distribution pattern of compression force on the earth of the tunnel excavation face is basically the same under different cutterhead opening ratios. That is, due to the disturbance of shield tunneling, the compression force of the earth within a range of about 1.2 D (D is tunnel diameter) on the excavation face is greater than that of the surrounding strata. Among them, the compression force of the earth around the cutterhead is greater, and the compression force of the earth at the center of the cutterhead is smaller. However, as the opening ratio of the cutterhead increases, the compressive force on the earth in front of the cutterhead gradually decreases, and the decrease is more pronounced at the center of the cutterhead. In addition, the compression force of the earth in the area where the cutterhead directly contacts the earth, such as the circumference and spokes, is significantly higher than that of the surrounding earth particles, indicating that as the cutterhead opening ratio decreases, the cutterhead's support effect on the earth in front becomes more pronounced.

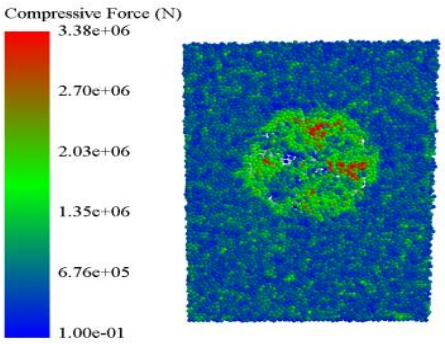

(a)

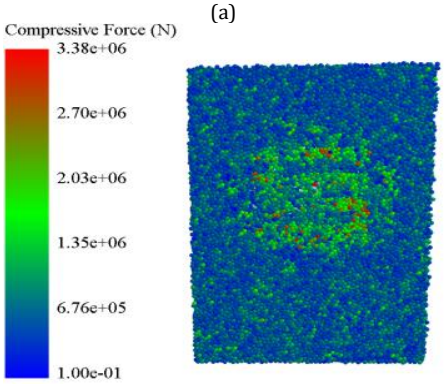

(b)

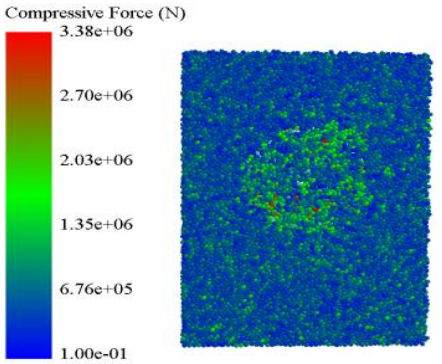

(c)

Fig. 9 Stress state of tunnel face under different cutterhead opening rates; (a) ψ =45%; (b) ψ =55%; (c) ψ =65%

The relationship between the horizontal displacement of the excavation face and the variation of the chamber earth pressure ratio under different cutterhead opening ratios is shown in Fig. 10.

From Fig. 10, the variation pattern of the horizontal displacement curve of the excavation face is basically consistent, showing the characteristics of large horizontal displacement in the upper part of the tunnel and small horizontal displacement in the lower part. The maximum horizontal displacement point appears in the upper center of the excavation face. As the cutterhead opening rate increases, the deformation of the excavation face increases, and the deformation curve of the excavation face fluctuates greatly, indicating poor stability of the excavation face. When the cutterhead opening ratio is 65%, the deformation in the middle of the excavation face is greater than that in the upper and lower parts, and the maximum horizontal displacement position of the excavation face is offset towards the upper part. This is due to the increase in the cutterhead opening ratio, which reduces the support area of the cutterhead on the front excavation face and reduces the stability of the excavation face earth. The cutterhead opening ratio has a significant impact on the stability of the tunnel excavation face. The critical chamber pressure ratios for cutterhead opening ratios of 45%, 55% and 65% are 0.26, 0.3 and 0.33, respectively, indicating that the required critical chamber pressure ratio for excavation increases with the increase of cutterhead opening ratio. This is because under the same chamber pressure ratio, as the pressure ratio decreases, the support effect of the chamber pressure on the excavation face becomes weaker. The stability of the excavation face depends more on the support of the cutterhead, while the cutterhead with a small opening ratio has a stronger support on the excavation face. Therefore, the critical chamber pressure ratio required to maintain the stability of the excavation face is lower.

The relationship between the maximum horizontal displacement of the excavation face and the chamber earth pressure under different cutterhead opening ratios is shown in Fig. 11.

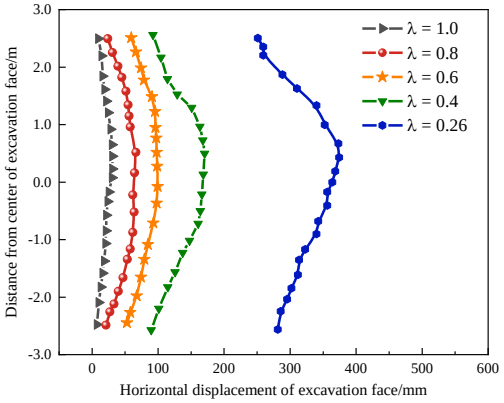

(a)

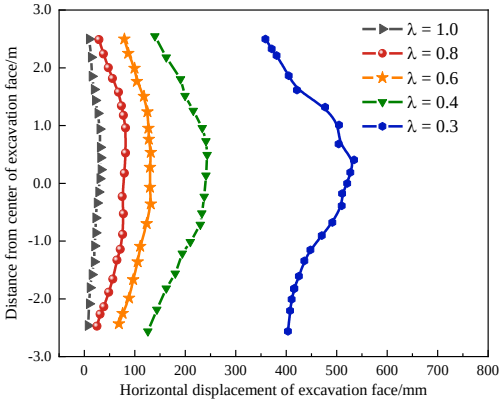

(b)

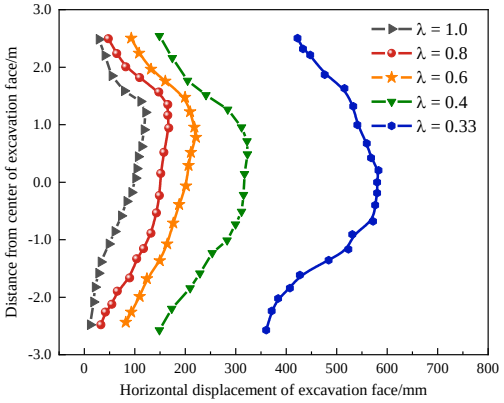

(c)

Fig. 10 Deformation of excavation face under different cutterhead opening rates; (a) ψ =45%; (b) ψ =55%; (c) ψ =65%

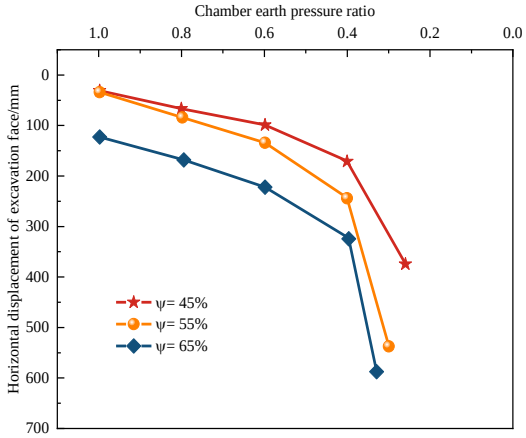

Fig. 11 Relationship between maximum horizontal displacement of excavation face and the chamber earth pressure at different cutterhead opening rates

As shown in Fig. 11, under the same chamber earth pressure ratio, the maximum horizontal displacement of the excavation face increases with the increase of the cutterhead opening ratio. As the pressure ratio decreases, the maximum horizontal displacement of the excavation face increases with the variation of the cutterhead opening rate, indicating that as the pressure ratio decreases, the maximum horizontal displacement of the excavation face is more sensitive to the variation of the cutterhead opening rate, and the influence of the cutterhead opening rate on the stability of the excavation face is greater. At the same chamber earth pressure, take the cutterhead opening rate of 45% and 55% as an example, the maximum horizontal displacement increases of the excavation face when the cutterhead opening rate changes from 45% to 55% is much smaller than when the cutterhead opening rate changes from 55% to 65%. Meanwhile, when the pressure ratio is 1 and the cutterhead opening ratio is 65%, the maximum horizontal displacement of the excavation face is 121.1 mm. At this point, the horizontal displacement of the excavation face is relatively large, and its stability is poor. Therefore, from the perspective of maintaining the stability of the excavation face, the cutterhead opening ratio should not be too large.

The ground subsidence curves of the stratum under different cutterhead opening ratios are shown in Fig. 12.

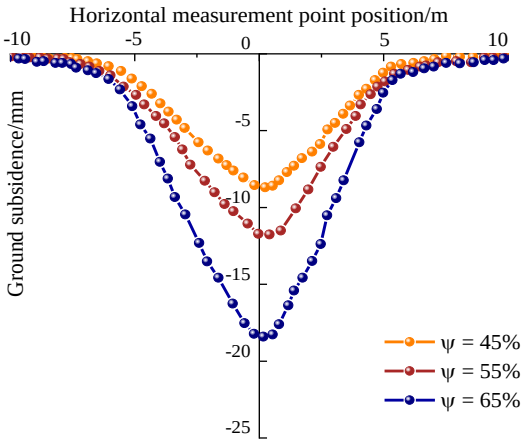

Fig. 12 Transverse ground settlement curve at different cutterhead opening rates

From Fig. 12, the settlement curve of the strata under different cutterhead opening rates is basically consistent, that is, the settlement curve of the strata follows a peck curve distribution, and the maximum settlement of the strata occurs near the centerline of the tunnel. The width of the settlement groove is less affected by the cutterhead opening rate. Meanwhile, the opening rate of the cutterhead has a significant impact on formation settlement. As the opening rate of the cutterhead increases, the amount of stratum settlement gradually increases. When opening rate ψ is 65%, the maximum subsidence of the strata is 18.53 mm, which is much greater than the maximum subsidence of the strata (8.59 mm) when the cutterhead opening rate ψ is 45%. This is due to the decrease in the cutterhead opening ratio, which leads to an increase in the area that the cutterhead can support, providing strong support for the earth ahead and enhancing the stability of the excavation face.

The excavation speed of shield tunneling is set at 30 mm/min, 60 mm/min and 90 mm/min, while other factors remain unchanged. The influence of excavation speed on the stability of the excavation face of shield tunneling is studied. The horizontal displacement of the excavation face varies with the chamber earth pressure at different tunnelling speeds, as shown in Fig. 13

As shown in Fig. 13, the deformation pattern of the excavation face is basically consistent under different tunnelling speeds, and the maximum horizontal displacement segment is located at the upper part of the tunnel centerline. As the speed of shield tunneling increases, the horizontal displacement of the excavation face also increases, but compared to factors such as tunnel burial depth and cutterhead opening rate, its increase is relatively small. When the pressure ratio of the chamber earth gradually decreases from 1 to 0.4, the horizontal displacement of the excavation face increases slightly, and the deformation curve of the excavation face is smoother. When the chamber earth pressure is further reduced to the critical pressure, the horizontal displacement of the excavation face increases sharply, and the deformation curve changes sharply. When the tunnelling speed is 90 mm/min, under the critical chamber earth pressure ratio, the deformation in the middle of the excavation face is relatively large, indicating that the shield machine will still cause excessive deformation of the excavation face at a faster excavation speed. To ensure the stability of the excavation face, the excavation speed should be controlled.

3.3 The influence of tunneling speed on the stability of excavation face

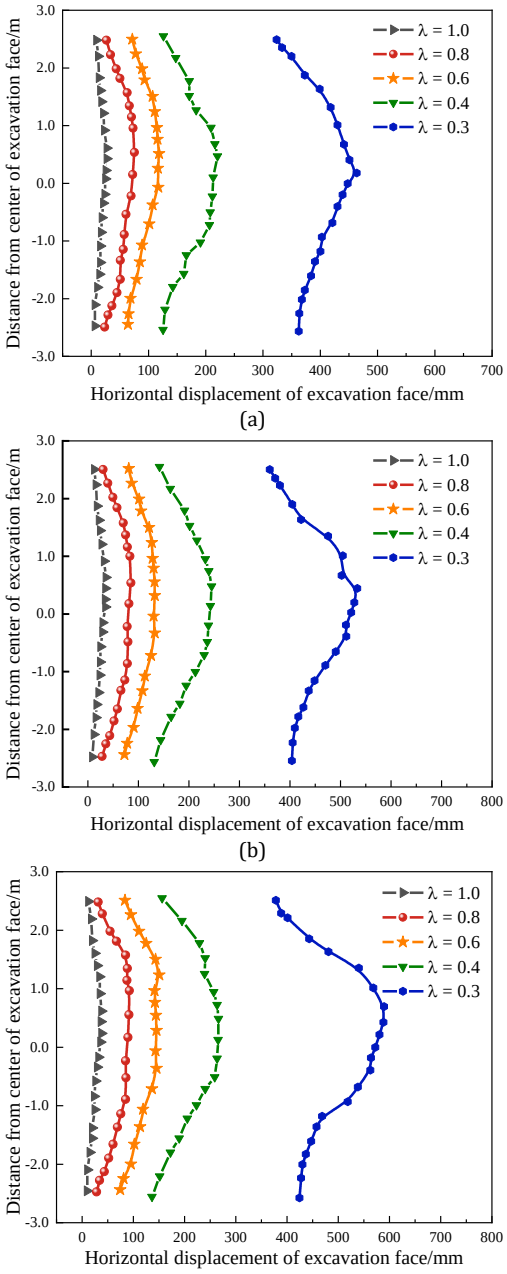

Fig. 13 Deformation of excavation face under different tunneling speeds; (a) v=30 mm/min; (b) v=60 mm/min; (c) v=90 mm/min.

The relationship between the maximum horizontal displacement of the excavation face and the chamber earth pressure under different excavation speeds is shown in Fig. 14.

As shown in Fig. 14, the maximum horizontal displacement of the excavation face increases with the increase of excavation speed, but the increase is small, and the difference in maximum horizontal displacement under the critical chamber earth pressure ratio is significant. As the pressure ratio decreases, the maximum horizontal displacement of the excavation face also shows a three-stage trend. The critical chamber earth pressure ratio at different excavation speeds is 0.3. In summary, the sensitivity of horizontal displacement of the excavation face to excavation speed is weaker than that of tunnel burial depth and cutterhead opening rate.

The settlement curves of the strata under different excavation speeds are shown in Fig. 15.

According to Fig. 15, the settlement curve of the strata under different excavation speeds is approximately distributed in a Peck curve. The closer to the centerline of the tunnel, the greater the settlement of the strata. The maximum settlement displacement of the strata at excavation speeds of 30 mm/min, 60 mm/min, and 90 mm/min are 6 mm, 12 mm, and 23 mm, respectively. This indicates that as the shield tunneling speed increases, the settlement of the strata also increases, and the width of the settlement groove also increases. The sensitivity of ground subsidence to excavation speed is greater than that of horizontal displacement of the excavation face, that is, the impact of changes in excavation speed on ground

subsidence is greater than that on horizontal displacement of the excavation face. Therefore, from the perspective of controlling the excavation face of the surrounding rock and the settlement of the strata, the lower the excavation speed of the shield tunnel, the more favorable it is for controlling the deformation of the surrounding rock.

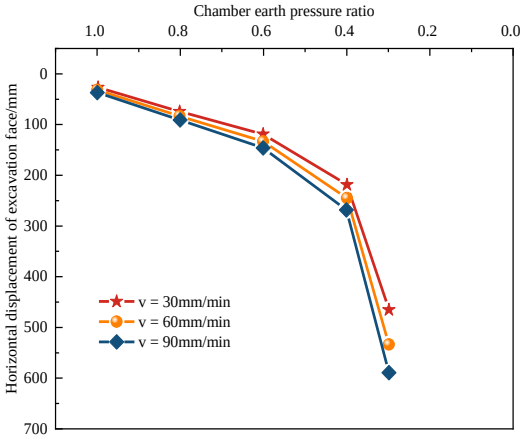

Fig. 14 Relationship between maximum horizontal displacement of excavation face and the chamber earth pressure at different tunnelling speeds

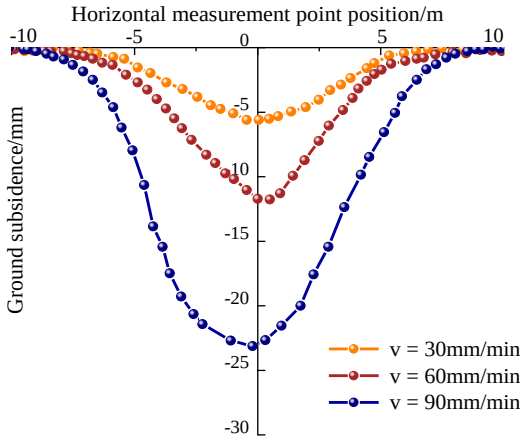

Fig. 15 Transverse ground settlement curve under different tunnelling speeds

3.4 The influence of cutterhead speed on the stability of excavation face

The speed of the shield tunneling cutterhead is set to 1 rpm, 3 rpm and 5 rpm, while keeping other factors constant. The influence of the cutterhead speed on the stability of the shield tunnel excavation face is studied. The relationship curve between the horizontal displacement of the excavation face and the speed of the cutterhead at different rotation rates is shown in Fig. 16.

From Fig. 16, under the same chamber earth pressure, when the cutterhead rotation rate is 1 rpm, the deformation of the middle part of the excavation face towards the chamber is relatively small, and the deformation curve of the excavation face is relatively flat. When the cutterhead rotation rate increases to 3 rpm and 5 rpm, the deformation of the middle part of the excavation face increases, and the curve fluctuates greatly. The horizontal displacement of the excavation face increases with the increase of the cutterhead speed, and the deformation in the middle of the excavation face is greater and thereby the curve fluctuates greatly. This is because the increase in the cutterhead rotation rate increases the frequency and degree of disturbance to the excavation face. The critical chamber earth pressure ratio under three different working conditions is 0.27, 0.3 and 0.32, respectively. That is, the critical pressure ratio increases with the increase of the cutterhead rotation rate. Overall, as the cutterhead speed increases, the stability of the excavation face decreases.

The relationship between the maximum horizontal displacement of the excavation face and the chamber earth pressure under different cutterhead rotation rates is shown in Fig. 17.

As shown in Fig. 17, under the same chamber earth pressure ratio, the maximum horizontal displacement of the excavation face increases with the increase of the cutterhead rotation rate, and the increase in the maximum horizontal displacement of the excavation face also gradually increases. When the pressure ratio is 1, the maximum horizontal displacement of the excavation face under three different working conditions is 30.81 mm, 43.54 mm, and 65.96 mm, with the maximum increase in horizontal displacement of 41.31% and 51.49%, respectively. As the pressure ratio decreases, the magnitude of the maximum horizontal displacement of the excavation face also increases continuously. In summary, during shield tunnel construction, even if the chamber earth pressure is controlled within a reasonable range, excessive cutterhead rotation rate will still lead to increased deformation of the excavation face, and the cutterhead speed has a greater impact on the deformation of the excavation face. The influence of cutterhead speed on the horizontal displacement of the excavation face is greater than that of excavation speed, but less than the cutterhead opening rate.

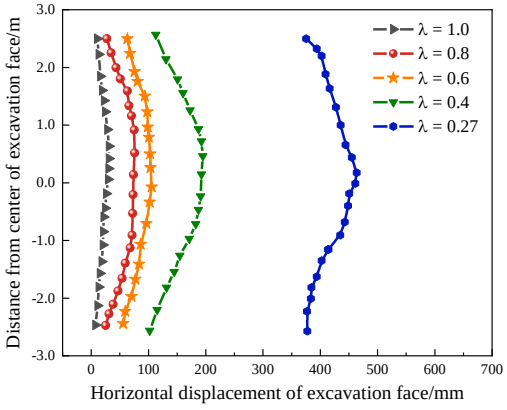

(a)

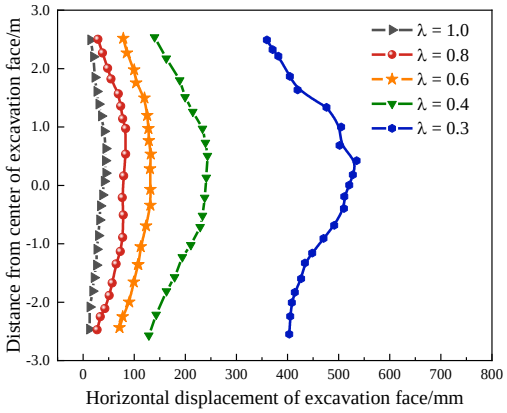

(b)

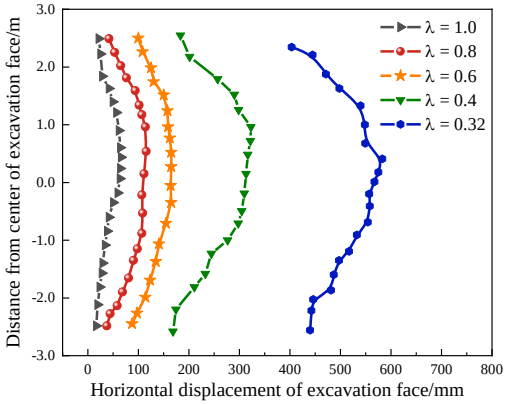

(c)

Fig. 16 Deformation of excavation face under different cutterhead rotation rates; (a) n=1 rpm; (b) n=3 rpm; (c) n=5 rpm.

The settlement curve of the strata under different cutterhead rotation rates is shown in Fig. 18.

From Fig. 18, the settlement curve of the strata still approximates the Peck curve at different cutterhead rotation rates. However, when the cutterhead speed is 1 rpm, there is an uplift phenomenon in the strata, with the maximum uplift starting point located about 6.5 m from the centerline of the tunnel and the maximum uplift of 3.13 mm. The reason for the uplift is that the rotational rate of the cutterhead does not match the tunnelling speed, resulting in compression of the earth in front of the cutterhead and causing uplift of the earth in front of the cutterhead. Meanwhile, as the speed of the cutterhead increases, the settlement of the formation also increases. The reason is that under the same working conditions, increasing the speed of the cutterhead increases the disturbance to the surrounding rock, and the deformation of the earth layer also increases. On a macro level, it is manifested that as the speed of the cutterhead increases, the settlement of the strata becomes more obvious. From the perspective of shield tunnel excavation safety, a smaller cutterhead speed is more beneficial for the stability of the excavation face,

but it affects the excavation speed. Therefore, the cutterhead speed should be determined by comprehensively considering the geology and construction conditions.

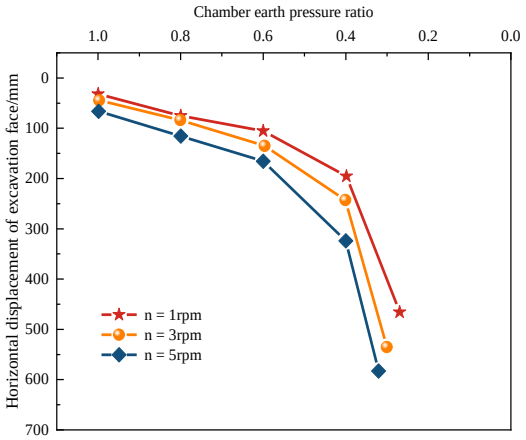

Fig. 17 Relationship between maximum horizontal displacement of excavation face and the chamber earth pressure under different cutterhead rotation rates

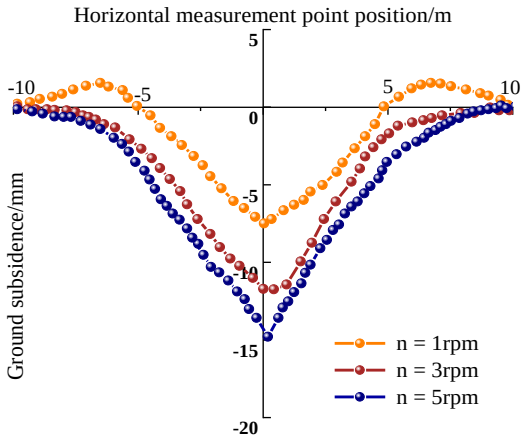

Fig. 18 Stratum settlement curves under different cutterhead rotation rates

4. Conclusions

Take the Bailuyuan Tunnel as an engineering case, a three-dimensional discrete element method was used to calibrate the microparameters of the rock and earth of the project site. The influence of tunnel burial depth, cutterhead opening ratio, excavation speed, and cutterhead rotation rate on the stability of the excavation face of the deep buried shield tunnel was studied, and the critical chamber earth pressure ratio of the shield tunnel under different factors was determined. The main conclusions are as follows:

(1) The horizontal displacement of the tunnel excavation face increases nonlinearly with the increase of tunnel burial depth, and the increase amplitude increases with the decrease of the chamber earth pressure ratio. With the increase of the buried depth of the tunnel, the critical chamber earth pressure ratio increases, the chamber earth pressure required to maintain the stability of the excavation surface gradually increases, and the stability of the excavation surface is worse.

(2) The horizontal displacement of the excavation face, geological settlement, and critical chamber earth pressure ratio all increase with the increase of the cutterhead opening rate. As the chamber earth pressure ratio decreases, the maximum horizontal displacement of the excavation face gradually increases with the increase of the cutterhead opening rate. With a large opening rate, the deformation of the excavation face in front of the cutterhead is more severe, while the cutterhead with a small opening rate can more effectively control the horizontal displacement and geological settlement of the excavation face, improving the stability of the excavation face.

(3) The horizontal displacement of the excavation face and the settlement of the strata increase with the increase of excavation speed and cutterhead rotation rate. The increasing extent of horizontal displacement of excavation face is stable. The increasing extent of ground settlement increases with the increase of tunneling speed and decreases with the increase of cutterhead speed. The critical chamber earth pressure ratio increases with the increase of cutterhead rotation rate but is not significantly affected by changes in excavation speed.

(4) Different factors have different impacts on the stability of the surrounding rock of shield tunnels. The burial depth has a significant impact on the horizontal displacement of the excavation face. The influence of cutterhead opening ratio and cutterhead rotation rate on the horizontal displacement of the excavation face is greater than on the settlement of the strata, while the influence of excavation speed on the strata settlement is greater than on the horizontal displacement of the excavation face.

Acknowledgements

The authors appreciate the Double first-class disciplines create engineering projects (AQ2024 0725).

Conflict of Interest

The authors declare that there is no conflict of interest regarding the publication of this paper.

References

Chen, L.Y., Wang, D. H., & Xu, J. (2022) Design optimization and construction control for the stability of shallow tunnels" by et al. International Journal of Civil Engineering.14,1238.

Chen, G. Y.,He, P., Xiao, J., & Bi, W. L.(2023) Study on Stability of Excavation Surface of Shield Tunnel in Clay Layer. Transportation Research Record, 2677 (12):675-693. https://doi.org/10.1177/03611981231169281

Di, Q. G., Li, P. F., Zhang, M. J., & Cui, X. P. (2023). Experimental study of face stability for shield tunnels in sandy cobble strata of different densities[J]. Tunnelling and Underground Space Technology incorporating Trenchless Technology Research, 135.

Dong, F., Fang, Q., Zhang, D. L., Xu, H. J., Li, Y. J., & Niu, X. K. (2017). Analysis on defects of operational metro tunnels in Beijing[J]. Journal of Civil Engineering, 50(06): 104-113.

Fu, X. S., Gong, Q. M., Wu, Y. J., Zhao, Y., & Li, H. (2022). Prediction of EPB shield tunneling advance rate in mixed ground condition using optimized BPNN model. Appl. Sci. 12, 5485. https://doi.org/10.3390/app12115485

Ge, S. S., Gao, W., Wang, Y. W., Xie, Y., Chen, X., & Wang, S. (2023). Review on evaluation and treatment of traffic shield tunnel defects in China[J]. Journal of Civil Engineering, 56(01): 119-128. https://dx.doi.org/10.15951/j.tmgcxb.21111120

Hernández, Y. Z., Farfán, A. D., & André. P. A. (2019) Three-dimensional analysis of excavation face stability of shallow tunnels, Tunnelling and Underground Space Technology, 92. https://dx.doi.org/10.1016/j.tust.2019.103062

Ibrahim, E., Soubra, A., Mollon, G., Raphael, W., Dias, D., & Reda, A. (2015). Three-dimensional face stability analysis of pressurized tunnels driven in a multilayered purely frictional medium[J]. Tunnelling and Underground Space Technology incorporating Trenchless Technology Research, 4918-34. https://dx.doi.org/10.1016/j.tust.2015.04.001

Lu, D. C., Ma, Y. D., Kong, F. C., Guo, C. X., Miao, J. B., & Du, X. L. (2023). Support vector regression with heuristic optimization algorithms for predicting the ground surface displacement induced by EPB shield tunneling[J]. Gondwana Research, 1233-15. https://dx.doi.org/10.1016/j.gr.2022.07.002

Li, S. Q., Zhang, Y. N., & Zhi, J. M. (2019) Influence of tunnel design and construction parameters on the stability of shallow tunnel faces. Tunnelling and Underground Space Technology.132(15):384-397.

Li, W., Zhang, C. P., Tu, S. Q., Chen, W., & Ma, M. S. (2023). Face stability analysis of a shield tunnel excavated along inclined strata, Underground Space, Volume 13, Pages 183-204, ISSN 2467-9674. https://dx.doi.org/10.1016/j.undsp.2023.03.007

Liu, X. R., Liu, D. S., Chen, Q., Zhou, X. H., & Xiong F. (2022). Research on the sensitivity of factors affecting the stability of slurry shield excavation face and control parameter optimization[J]. Chinese Journal of Underground Space and Engineering, 18(06): 1954-1961.

Liang, Q., Xu, J. J., & Wei, Y. G. (2023). Three-dimensional stability analysis of tunnel face based on unified strength theory. Sci Rep 13, 12326.

Niu, Y. L., Ren, T. L., Zhou, Q., & Jiao, X. Y. (2023) Analysis of excavation parameters on face stability in small curvature shield tunnels. Sustainability, 15, 6797. https://dx.doi.org/10.1038/s41598-023-39554-z

Su, A., Wang, S. M., He, C., Lu, D. Y., & Fang, R. Q. (2019). Disease characteristics and causes analysis of segments of shield tunnels incomposite stratum during construction[J]. Chinese Journal of Geotechnical Engineering, 41(04): 683-692.

Wang, L., Ren, K.F., & Yang, S.Y. (2023) Stability analysis of shallow tunnels considering the interaction between design and construction factors. Journal of Rock Mechanics and Geotechnical Engineering.13(02):527-536.

Xu, Q. W., Xie, J. L., & Zhang, L. Y. (2023) Failure analysis of progressive instability and deformation law of excavation face in sand cobble stratum under cutting disturbance by shield cutter, Engineering Failure Analysis, volume 154. https://dx.doi.org/10.1016/j.engfailanal.2023.107711

Yao, Q. Y., Zhang, R. L., Gong, Q. M., & Zhou, S. H. (2023). Analysis of shield Excavation face failure and tunneling control with two parameters in sandy cobble strata[J]. Journal of Tongji University (Natural Science), 51(09): 1407-1415. https://dx.doi.org/10.11908/j.issn.0253-374x.22460

Yang, Z. N., Liu, Q. W., & Liu, L. S. (2016). Sensitivity analysis of factors affecting the stability of slurry shield excavation face [J]. Modern tunnel technology, 53(02): 141-147. https://dx.doi.org/10.13807/j.cnki.mtt.2016.02.020

Zhang, J. X., Li, B., Jiang, Y. S., Jiang, H., Yin, M. L., & Sun, Z. Y. (2023). Research on the wear characteristics of shield cutter in sand-pebble strata based on EDEM[J]. Chinese Journal of Geotechnical Engineering: 4: 1-8.

Zhang, Z. Q., Li, H. Y., & Yang, H. Y. (2019) Failure modes and face instability of shallow tunnels under soft grounds, International Journal of Damage Mechanics,28(4):566-589. https://dx.doi.org/10.1177/1056789518773135

Disclaimer